

Control of Overpopulated Tails in Kinetic Epidemic Models

M. Zanella^{*} A. Medaglia[†]

January 10, 2025

Abstract

We introduce model-based transition rates for controlled compartmental models in mathematical epidemiology, with a focus on the effects of control strategies applied to interacting multi-agent systems describing contact formation dynamics. In the framework of kinetic control problems, we compare two prototypical control protocols: one additive control directly influencing the dynamics and another targeting the interaction strength between agents. The emerging controlled macroscopic models are derived for an SIR compartmentalization to illustrate their impact on epidemic progression and contact interaction dynamics. Numerical results show the effectiveness of this approach in steering the dynamics and controlling epidemic trends, even in scenarios where contact distributions exhibit an overpopulated tail.

1 Introduction

In this work, we focus on the derivation of model-based transition rates for controlled compartmental models in mathematical epidemiology, emphasizing the impact of a centralized control strategy applied to interacting multiagent systems describing contact formation dynamics. Control methods in compartmental epidemiology have been extensively studied to define optimal model-oriented non-pharmaceutical interventions over variable time horizons [5, 6, 10, 22, 24, 39, 47]. Further approaches have focused on control methods to optimize vaccination procedures and quarantine measures, see, e.g., [7, 13, 15, 23, 25, 32]. In this direction, the problem of controlling multiagent systems has recently emerged as a natural follow-up to the description and modeling of their self-organizing features [3, 8, 16, 17, 21]. In the case of large systems, significant

^{*}Department of Mathematics "F. Casorati", University of Pavia, Italy.
Email:mattia.zanella@unipv.it

[†]Mathematical Institute, University of Oxford, United Kingdom.
Email:andrea.medaglia@maths.ox.ac.uk

contributions have been made in the context of the derivation of control strategies for mean-field and kinetic equations, see, e.g., [1, 2, 4, 33, 34, 45] and the references therein.

The evolution of epidemics can be understood as the result of unobservable interactions among a large number of agents of heterogeneous populations, whose transitions are influenced by multidimensional factors, including both behavioural aspects and the biological characteristics of the pathogen [26, 30, 31, 36, 37, 40, 46]. In this context, kinetic theory emerges as a robust mathematical framework to understand the emerging statistical properties of large multiagent systems [12, 14, 19, 27, 28, 48]. A key motivation for introducing kinetic-type equations lies in their multiscale features, which connects the microscopic level of individual agents, where fundamental interactions occur, to the macroscopic level, where data are typically available. This characteristic links the kinetic approach to the effective evolution of multiagent systems. Moreover, the ability to derive macroscopic models that are consistent with the underlying microscopic interaction dynamics is crucial for parameter estimation, which in turn supports effective decision-making processes. In this context, we refer to [29, 35, 49] for comparisons of these modelling approaches with structured real data, particularly with respect to demographic factors such as age.

In this work, we focus on a kinetic model for epidemic dynamics in which the population of agents is divided into compartments and the mass of each compartment changes in connection with microscopic dynamics defining the emerging contact distribution of the system which characterises the heterogeneity of the population [11, 12, 41, 50]. The dynamics of the particles are governed by a simple transition operator consistent with growth-type operators [44, 48]. At the kinetic level, this model may lead to the emergence of an equilibrium distribution characterized by a power-law tail.

Furthermore, we consider an instantaneous control of a contact-based dynamics with the minimization of a cost functional recently proposed in [29, 35] that provides a measure of the expected number of contacts of an agent. In particular, we consider instantaneous controls that are active through the single step defining the microscopic agent-based transition. This leads to a feedback-type control problem which can be solved explicitly. The resulting control is then obtained in terms of the microscopic states of the interacting particles and then embedded in a Boltzmann-type kinetic description of large agent systems. This strategy has been proposed in connection with model predictive control (MPC) approaches and applied to space-homogeneous multiagent systems, see [4] and the references therein. The approach has been further extended to kinetic space non-homogeneous models, see, e.g., [20, 45].

In the framework of kinetic control problems, we consider two control strategies aimed at influencing the dynamics of the multiagent system. The first approach employs an additive control mechanism that directly modifies the agents' individual dynamics, while the second targets the interaction strength between agents, effectively shaping the overall interaction structure. By deriving the corresponding controlled macroscopic models, we apply these strategies to an SIR compartmentalization of the society. This allows us to investigate their

impact on both the progression of an epidemic and the dynamics of contact interactions within the population. The comparison highlights that controlling the interaction is capable of influencing the nature of the contact structure of agents by shaping the tail of the contact distribution.

In more detail, the present paper is organised as follows. In Section 2 we recall basic concepts of kinetic modelling for epidemic dynamics, and the emerging equilibrium densities of contact formation dynamics have been obtained. Hence, in Section 2.2-2.3 we embed the obtained equilibrium density in the kinetic model to derive the evolution of observable quantities. The control of the tail behaviour is discussed in Section 3 by comparing two control strategies. In Section 3.1 the emerging distributions of the resulting Fokker-Planck equations for the two control protocols are computed and compared, and the macroscopic equations are obtained in Section 3.2. Finally, in Section 4 we present several numerical results.

2 Kinetic compartmental models with contact structure

We consider a prototypical system of agents subdivided into the following epidemiological relevant states: susceptible (S) agents are the ones that can contract the disease, infected and infectious, (I) agents are responsible for the spread of the disease, and removed (R) agents cannot spread the disease. In the following, we will indicate with $\mathcal{C} = \{S, I, R\}$ the considered compartmentalization of the population.

We denote by $f_J = f_J(x, t) : \mathbb{R}^+ \times \mathbb{R}^+ \rightarrow \mathbb{R}^+$, $J \in \mathcal{C}$, the distribution of the number of contacts $x \in \mathbb{R}^+$ at time $t \geq 0$ of agents in the compartment $J \in \mathcal{C}$. Hence, the contact distribution $f(x, t)$ of the society is obtained as follows

$$\sum_{J \in \mathcal{C}} f_J(x, t) = f(x, t), \quad \int_{\mathbb{R}^+} f(x, t) dx = 1,$$

and the mass fractions of the population in each compartment are defined as

$$\rho_J(t) = \int_{\mathbb{R}^+} f_J(x, t) dx,$$

while their moment of order $r > 0$ are given by

$$\rho_J(t) m_{r,J}(t) = \int_{\mathbb{R}^+} x^r f_J(x, t) dx.$$

In the following, we discuss the evolution of the contact distributions $f_J(x, t)$ due to microscopic interactions.

2.1 Contact formation dynamics

We consider a large system of $N \gg 0$ agents that are identified by their number of daily contacts $x_i \in \mathbb{R}^+$, $i = 1, \dots, N$. The dynamics of each agent is modified

through deterministic variations of the contact structure due to environmental factors, and by random fluctuations in the contact variation due to population heterogeneities. Following the approach presented in [28] and indicating by x' the post-interaction number of contacts of an agent, we get

$$x' = x + \epsilon \frac{\alpha}{2\delta} \left(\left(\frac{x}{m_J} \right)^\delta - 1 \right) x + x\eta, \quad (1)$$

where $\Psi(x) = \frac{\alpha}{2\delta} \left(\left(\frac{x}{m_J} \right)^\delta - 1 \right)$ is a generic growth function which describes logistic-type growths for any $\delta > 0$, von Bertalanffy-type growths for $\delta < 0$ and coincides with a Gompertz growth function in the limit $\delta \rightarrow 0$, see [44]. In (1), we further introduced the random variable η such that, denoting by $\langle \cdot \rangle$ the expectation with respect to the distribution of the introduced r.v., we get $\langle \eta \rangle = 0$ and $\langle \eta^2 \rangle = \epsilon \sigma^2$.

Hence, following the approach in [18, 42], we can characterise the contact formation dynamics for the generic compartment $f_J = f_J(x, t)$ by considering the following space homogeneous Boltzmann-type equation

$$\frac{\partial}{\partial t} f_J(x, t) = \left\langle \int_{\mathbb{R}^+} B(x) \left(\frac{1}{'J} f_J('x, t) - f_J(x, t) \right) dx \right\rangle, \quad (2)$$

where $'x \geq 0$ denote the pre-transition number of contacts that produces the post-transition contacts $x \geq 0$ following the transition scheme (1), while $'J$ denotes the determinant of the Jacobian of the transformation $'x \rightarrow x$. In (2), the term $B(x) : \mathbb{R}^+ \rightarrow \mathbb{R}^+$ is the collision kernel tuning the interaction frequency which may depend on the number of contacts $x \geq 0$. In [35], the kernel

$$B(x) = x^{-\frac{1+\delta}{2}},$$

has been considered. The kinetic equation (2) can be conveniently written in weak form by introducing a test function $\varphi(\cdot)$. Hence, the evolution of observable quantities is given as follows

$$\frac{d}{dt} \int_{\mathbb{R}^+} \varphi(x) f_J(x, t) dx = \int_{\mathbb{R}^+} B(x) \langle \varphi(x') - \varphi(x) \rangle f_J(x, t) dx.$$

The introduced operator is always mass preserving: by choosing $\varphi(x) = 1$ we get

$$\int_{\mathbb{R}^+} Q_J(f_J)(x, t) dx = 0.$$

It is momentum-preserving if $\delta \equiv \pm 1$ since from (7) we get

$$\int_{\mathbb{R}^+} x Q_J(f_J)(x, t) dx = -\frac{\alpha}{2\delta} \int_{\mathbb{R}^+} x^{1-\frac{1+\delta}{2}} \left(\left(\frac{x}{m_J} \right)^\delta - 1 \right) f_J(x, t) dx.$$

More generally, for any $\delta \in (-1, 1)$ the momentum is not a conserved quantity for the introduced collision operator.

In view of the complexity of obtaining an analytical expression on the large time behaviour of the kinetic equation (7), it is possible to derive from the introduced kinetic model a reduced complexity Fokker-Planck-type partial differential equation for which the study of asymptotic properties is easier, see [42]. In the quasi-invariant limit, we get the following operator

$$\bar{Q}_J(f_J)(x, t) = \frac{\alpha}{2\delta} \partial_x \left[x^{1-\frac{1+\delta}{2}} \left(\left(\frac{x}{m_J} \right)^\delta - 1 \right) f_J + \frac{\sigma^2}{2} \partial_x \left(x^{2-\frac{1+\delta}{2}} f_J \right) \right]. \quad (3)$$

For the sake of brevity, we omit here the details of the derivation, we point the interested reader to [28] for more details. We can observe how the derived Fokker-Planck operator $\bar{Q}_J(\cdot)$ is mass preserving and momentum preserving if $\delta = \pm 1$.

Remark 2.1. *The process defined in (1) can be obtained in terms of a system of stochastic differential equations (SDEs) for the dynamics of each agent of the system $\{x_i\}_{i=1}^N$ where the dynamics characterising the number of contacts of each agent is described as follows*

$$dx_i = B(x_i)\Psi(x_i)dt + \sqrt{2\sigma^2 x_i}dW_i^t,$$

being $\{W_i^t\}_{i=1}^N$ a set of independent Wiener processes and $B(x_i) \geq 0$ a factor describing the interaction frequency of each agent, see [48]. Following [38] it can be shown that in the limit $N \rightarrow +\infty$ the evolution of the system of agents is obtained in terms of the evolution of a probability density solution to the Fokker-Planck equation (3).

2.1.1 Equilibrium distribution of the Fokker-Planck equation

The Fokker-Planck-type operator defined in (3) is such that its equilibrium density $f_J^q(x)$ can be computed as the unique solution to the following differential equation

$$\frac{\mu}{\delta} x^{1-\frac{1+\delta}{2}} \left(\left(\frac{x}{m_J} \right)^\delta - 1 \right) f_J^q(x) + \sigma^2 \partial_x \left(x^{2-\frac{1+\delta}{2}} f_J^q(x) \right) = 0, \quad \delta \in [-1, 1]$$

which is given by

$$f_J^q(x) = C_{\delta, \sigma^2, \alpha} x^{-\frac{\alpha}{\sigma^2 \delta} - 2 + \frac{1+\delta}{2}} \exp \left\{ -\frac{\alpha}{\sigma^2 \delta^2} \left(\frac{x}{m_J} \right)^\delta \right\}, \quad (4)$$

where $C_{\delta, \mu, \sigma^2} > 0$ is a normalization constant.

The equilibrium solution obtained in (4) depends on the parameter $\delta \in [-1, 1]$ of the model which influences the behaviour of the tails. Indeed, we may observe how, for any $0 \leq \delta \leq 1$ the equilibrium distribution is characterized by

slim tails since it exhibits exponential decay for $x \gg 0$. In particular, in the case $\delta = 1$ we get a Gamma distribution

$$f_J^q(x) = \frac{\lambda^\lambda}{m_J^\lambda \Gamma(\lambda)} x^{\lambda-1} \exp\left\{-\frac{\lambda x}{m_J}\right\}, \quad \lambda = \frac{\alpha}{\sigma^2}, \quad (5)$$

having slim tails. In the case of the Gamma distribution, we have the following relations on the first and second order moment

$$\int_{\mathbb{R}^+} x f_J^q(x) dx = m_J, \quad \int_{\mathbb{R}^+} x^2 f_J^q(x) dx = \frac{\lambda+1}{\lambda} m_J^2.$$

Furthermore, in the special case $\delta \rightarrow 0$ it can be shown that the equilibrium density is a lognormal distribution [44]. On the other hand, for any $\delta < 0$ the equilibrium distribution is a fat tails distribution with polynomial decay for $x \gg 0$. In particular, if $\delta = -1$, we obtain the inverse Gamma distribution

$$f_J^q(x) = \frac{(\lambda m_J)^{\lambda+1}}{\Gamma(\lambda+1)} x^{-2-\lambda} \exp\left\{-\frac{\lambda m_J}{x}\right\}, \quad \lambda = \frac{\alpha}{\sigma^2}, \quad (6)$$

for which we have

$$\int_{\mathbb{R}^+} x f_J^q(x) dx = m_J, \quad \int_{\mathbb{R}^+} x^2 f_J^q(x) dx = \frac{\lambda}{\lambda-1} m_J^2.$$

Therefore, the sign of the generally unknown parameter $\delta \in [-1, 1]$ have a strong impact in terms of the behaviour of the multi-agent system.

2.2 Kinetic models model for epidemic spreading

Following the approach presented in [28], we are interested in the evolution of the kinetic densities $(f_J)_{J \in \mathcal{C}}$ solution to

$$\begin{cases} \partial_t f_S(x, t) = -K(f_S, f_I)(x, t) + \frac{1}{\tau} Q_S(f_S)(x, t), \\ \partial_t f_I(x, t) = K(f_S, f_I)(x, t) - \gamma_I f_I(x, t) + \frac{1}{\tau} Q_I(f_I)(x, t), \\ \partial_t f_R(x, t) = \gamma_I f_I(x, t) + \frac{1}{\tau} Q_R(f_R)(x, t), \end{cases} \quad (7)$$

where $\gamma_I > 0$ is the recovery rate. In (7), the transmission of the infection is governed by the local incidence rate

$$K(f_S, f_I)(x, t) = f_S(x, t) \int_{\mathbb{R}^+} \kappa(x, x_*) f_I(x_*, t) dx_*, \quad (8)$$

being $\kappa(x, x_*)$ the contact function weighting the frequency of contacts between susceptible and infected agents. We highlight that the case $\kappa(x, x_*) \equiv \beta > 0$ corresponds to the hypothesis of a homogeneous transmission between agents as

in the classical SIR model. To take into account the influence of the shape of the contact distribution of infected in the transmission dynamics we may consider

$$\kappa(x, x_*) = \sum_{\ell=1}^L \beta_{\ell} (xx_*)^{\ell}, \quad (9)$$

where $\beta_{\ell} \geq 0$ are proportionality parameters, and $\ell = 1, \dots, L$ determines the relevant moments of the contact distribution in the infection dynamics. In [28], the case $L = 1$ has been considered, for which the mean number of connections of the infected population weights the spread of the infection. In this case we get

$$K(f_S, f_I)(x, t) = -\beta_1 x f_S \rho_I m_I.$$

More generally, higher order moments of the distribution are necessary to characterize the spread of the infection. To understand the impact of the tails of the contact distribution, we can consider the case $L = 2$. Hence, under this hypothesis the incidence rate defined in (8) reads

$$K(f_S, f_I)(x, t) = \beta_1 x f_S(x, t) \rho_I(t) m_{1,I}(t) + \beta_2 x^2 f_S(x, t) \rho_I m_{2,I}(t).$$

In this case, we obtain information on the impact of the mean and energy of the contact distribution on the evolution of the disease. Within the choice in (9), the incidence rate is proportional to the product of the mean number of contact of susceptible and infected agents and on their energies.

2.3 Macroscopic equations

In this section, we derive the evolution of observable quantities of the kinetic system of equations (7). In Section 2.1.1 we have observed how the conserved quantities of the contact formation dynamics are given by mass and momentum, for which we wish to obtain a closed system of equations describing their evolution. In the following, we introduce an approximation which is reminiscent of the equilibrium closure in classical kinetic theory, see e.g. [9].

As observed in [48], under the hypothesis $\kappa(x, x_*) \equiv \beta$, corresponding to the case where the infection dynamics is independent from the contact distribution, we obtain a system defining the evolution of mass fractions given by the classical SIR model. Indeed, integrating (7) in \mathbb{R}^+ we get

$$\begin{aligned} \frac{d}{dt} \rho_S &= -\beta \rho_S \rho_I, \\ \frac{d}{dt} \rho_I &= \beta \rho_S \rho_I - \gamma_I \rho_I, \\ \frac{d}{dt} \rho_R &= \gamma_I \rho_I \end{aligned}$$

whereas from (7) we may compute $1/\rho_J(t) \int_{\mathbb{R}_+} x f_J(x, t) dx$ from which we get $\frac{d}{dt} m_J(t) = 0$ for all $J \in \mathcal{C}$. A first attempt to incorporate the impact of social

contacts in the dynamics is obtained by choosing $L = 1$ from which we get

$$\begin{aligned}\frac{d}{dt}\rho_S &= -\beta_1\rho_S m_{1,S}\rho_I m_{1,I}, \\ \frac{d}{dt}\rho_I &= \beta_1\rho_S m_{1,S}\rho_I m_{1,I} - \gamma_I\rho_I, \\ \frac{d}{dt}\rho_R &= \gamma_I\rho_I,\end{aligned}\tag{10}$$

such equation can be coupled with the evolution of the mean number of connections which is a conserved quantity of the collision operator (3). We get

$$\begin{aligned}\frac{d}{dt}\rho_S m_{1,S} &= -\beta_1\rho_S m_{2,S}\rho_I m_{1,I}, \\ \frac{d}{dt}\rho_I m_{1,I} &= \beta_1\rho_S m_{2,S}\rho_I m_{1,I} - \gamma_I\rho_I m_{1,I}, \\ \frac{d}{dt}\rho_R m_{1,R} &= \gamma_I\rho_I m_{1,I}.\end{aligned}\tag{11}$$

In view of the fact that the equilibrium distribution of the operator (3) is either a Gamma distribution, if $\delta = 1$, or an inverse Gamma distribution, if $\delta = -1$, in the limit $\tau \rightarrow 0^+$, we have the following equilibrium closure

$$\int_{\mathbb{R}_+} x^2 f_S(x, t) dx \approx \int_{\mathbb{R}_+} x^2 \rho_S(t) f_S^q(x, t) dx = \begin{cases} \frac{\lambda + 1}{\lambda} \rho_S m_S^2 & \delta = 1 \\ \frac{\lambda}{\lambda - 1} \rho_S m_S^2 & \delta = -1. \end{cases}\tag{12}$$

being $\lambda = \alpha/\sigma^2$. Hence, we may couple the evolution of mass fractions with the evolution of the first order moment which, in its closed form reads

$$\begin{aligned}\frac{d}{dt}m_{1,S} &= -\beta_1 m_{1,S}^2 \rho_I m_{1,I} (\Lambda - 1), \\ \frac{d}{dt}m_{1,I} &= \beta_1 \rho_S m_{1,S} m_{1,I} (\Lambda m_{1,S} - m_{1,I}), \\ \frac{d}{dt}m_{1,R} &= \gamma_I \frac{\rho_I}{\rho_R} (m_{1,I} - m_{1,R}),\end{aligned}\tag{13}$$

being $\Lambda = ((\lambda + \delta)/\lambda)^\delta > 1$ for any $\delta = \pm 1$. The evolution of mass fractions (10), coupled with the closed evolution of first order moments (13), forms a new system of macroscopic equations that inherits the properties of the microscopic agent-based system describing the dynamics of contact formation. The evolution of the mean number of contacts of the susceptible population is always decreasing in time, therefore the maximum number of contacts of the infected population is

$$\bar{m}_{1,I} = \begin{cases} \frac{\lambda + 1}{\lambda} m_{1,S}(0) & \delta = 1, \\ \frac{\lambda}{\lambda - 1} m_{1,S}(0) & \delta = -1. \end{cases}\tag{14}$$

Furthermore, we can observe that

$$\bar{m}_{1,I}^{(\delta=-1)} > \bar{m}_{1,I}^{(\delta=1)},$$

and the number of contacts of the infected population corresponding to an inverse Gamma closure ($\delta = -1$) are higher compared to the number of contacts obtained with a Gamma closure ($\delta = 1$).

Consistently with the closure that we obtained, as $\lambda \rightarrow +\infty$, which means $\sigma^2 \rightarrow 0^+$, the two models describe the same trajectory. It is worth to observe that, if $\sigma \rightarrow 0^+$, we get a population with no contact heterogeneities and, therefore, we collapse to the standard SIR model. In other words, the classical SIR model can be obtained through a Dirac delta closure centered on the mean m_J . In Figure 1 we depict the epidemic trajectories for several $\sigma^2 = 0.2, 0.4$ and fixed $\alpha = 1$, in all cases we considered as initial condition $m_J(0) = 10$ and $\rho_I(0) = \rho_R(0) = 10^{-3}$, $\rho_S(0) = 1 - \rho_I(0) - \rho_R(0)$. We may observe that for larger λ the model obtained with inverse Gamma closure provides a higher mean number of contacts for the infected population.

Finally, in the case $L = 2$ the evolution of the masses reads

$$\begin{aligned} \frac{d}{dt}\rho_S &= -\beta_1\rho_S m_{1,S}\rho_I m_{1,I} - \beta_2\rho_S m_{2,S}\rho_I m_{2,I} \\ \frac{d}{dt}\rho_I &= \beta_1\rho_S m_{1,S}m_{1,I}\rho_I + \beta_2 m_{2,S}\rho_S\rho_I m_{2,I} - \gamma_I\rho_I \\ \frac{d}{dt}\rho_R &= \gamma_I\rho_I \end{aligned} \quad (15)$$

which can be coupled with the evolution of the mean number of contacts

$$\begin{aligned} \frac{d}{dt}\rho_S m_{1,S} &= -\beta_1\rho_S m_{2,S}\rho_I m_{1,I} - \beta_2\rho_S m_{3,S}\rho_I m_{2,I} \\ \frac{d}{dt}\rho_I m_{1,I} &= \beta_1\rho_S m_{2,S}\rho_I m_{1,I} + \beta_2\rho_S m_{3,S}\rho_I m_{2,I} - \gamma_I\rho_I m_{1,I} \\ \frac{d}{dt}\rho_R m_{1,R} &= \gamma_I\rho_I m_{1,I}. \end{aligned} \quad (16)$$

As before, in the limit $\tau \rightarrow 0^+$ we can obtain a closed evaluation of higher order moments through an equilibrium closure approach, i.e. by exploiting the information in (5) and (6) for $J \in \{S, I\}$

$$\begin{aligned} \int_{\mathbb{R}} x^2 f_J(x, t) dx &\approx \int_{\mathbb{R}} x^2 f_J^\infty(x, t) dx = \begin{cases} \frac{\lambda+1}{\lambda} \rho_J m_J^2 & \delta = 1 \\ \frac{\lambda}{\lambda-1} \rho_J m_J^2 & \delta = -1, \end{cases} \\ \int_{\mathbb{R}} x^3 f_J(x, t) dx &\approx \int_{\mathbb{R}} x^3 f_J^\infty(x, t) dx = \begin{cases} \frac{(\lambda+1)(\lambda+2)}{\lambda^2} \rho_J m_J^3 & \delta = 1 \\ \frac{\lambda^2}{(\lambda-1)(\lambda-2)} \rho_J m_J^3 & \delta = -1. \end{cases} \end{aligned} \quad (17)$$

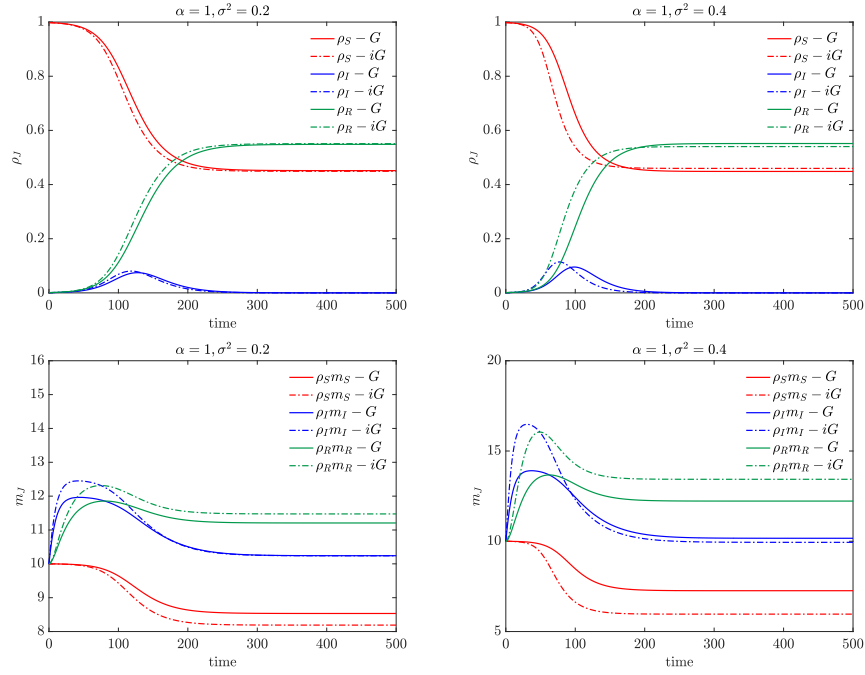


Figure 1: **Case $L = 1$:** Epidemic trajectories of the system (10)-(11) with closure (12). The continuous line corresponds to the evolution of the system obtained with a Gamma closure and the dashdotted line the evolution of the system with inverse Gamma closure. As initial condition we considered as initial condition $m_J(0) = 10$, $J \in \mathcal{C}$, and $\rho_I(0) = \rho_R(0) = 10^{-5}$, $\rho_S(0) = 1 - \rho_I(0) - \rho_R(0)$ and $\beta_1 = 10^{-3}$, $\gamma_I = 1/14$. From left to right we present the cases $\lambda = 5$ (left), $\lambda = 2.5$ (right).

For fat-tailed distributions, the obtained closure is derived under the condition that $\lambda > 2$, i.e., $\frac{\alpha}{\sigma^2} > 2$, as the third order moment must be well-defined. Hence, in the limit $\tau \rightarrow 0^+$ the evolution of mass fractions reads

$$\begin{aligned}\frac{d}{dt}\rho_S &= -\beta_1\rho_S m_{1,S}\rho_I m_{1,I} - \Lambda^2\beta_2\rho_S m_{1,S}^2\rho_I m_{1,I}^2 \\ \frac{d}{dt}\rho_I &= \beta_1\rho_S m_{1,S}m_{1,I}\rho_I + \beta_2\Lambda^2\rho_S m_{1,S}^2\rho_I m_{1,I}^2 - \gamma_I\rho_I \\ \frac{d}{dt}\rho_R &= \gamma_I\rho_I\end{aligned}\quad (18)$$

which is coupled to the following system for the evolution of the mean number of contacts

$$\begin{aligned}\frac{d}{dt}m_{1,S} &= -m_{1,S}^2\rho_I m_{1,I} \left(\frac{2\beta_1}{2\lambda - 1 + \delta} + 2\beta_2 \left(\frac{\lambda + \delta}{\lambda} \right)^{2\delta} \frac{1}{\lambda - 1 + \delta} m_{1,S}m_{1,I} \right) \\ \frac{d}{dt}m_{1,I} &= \rho_S m_{1,S}m_{1,I} \left[\beta_1 (\Lambda m_{1,S} - m_{1,I}) + \beta_2 \Lambda^2 \left(\left(\frac{\lambda + 2\delta}{\lambda} \right)^\delta m_{1,S} - m_{1,I} \right) m_{1,S}m_{1,I} \right], \\ \frac{d}{dt}m_{1,R} &= \gamma_I \frac{\rho_I}{\rho_R} (m_{1,I} - m_{1,R}),\end{aligned}\quad (19)$$

being $\Lambda = ((\lambda + \delta)/\lambda)^\delta > 1$ with $\delta = \pm 1$. As in the case $L = 1$, the mean number of contacts of the susceptible population decreases in time whereas, focussing only on the effects of the second order moments, if $\beta_1 = 0$ the maximum number of contacts of the infected population is given by

$$\hat{m}_{1,I} = \begin{cases} \frac{\lambda + 2}{\lambda} m_{1,S}(0) & \delta = 1 \\ \frac{\lambda}{\lambda - 2} m_{1,S}(0) & \delta = -1, \end{cases}\quad (20)$$

and we have the following order relation between the obtained maxima in (20)

$$\hat{m}_{1,I}^{(\delta=-1)} > \hat{m}_{1,I}^{(\delta=1)},$$

for any $\lambda > 0$. Hence, the infected population reaches a higher number of contacts in the presence of power-law tails. Furthermore, the obtained maxima for $L = 1$ in (14) and $L = 2$ in (20) are such that

$$\bar{m}_{1,I}^{(\delta=-1)} < \hat{m}_{1,I}^{(\delta=-1)}.$$

Therefore, the model obtained with taking into account higher order moments produces higher maximum in the mean number of contacts of infected population.

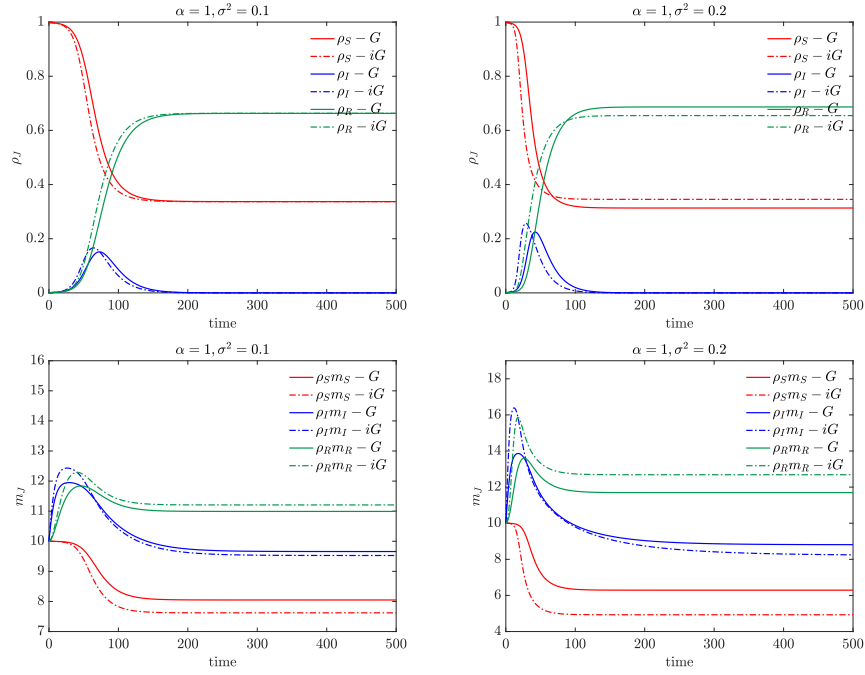


Figure 2: **Case $L = 2$** : Epidemic trajectories of the system (18)-(19) with closure discussed in (17). The continuous line corresponds to the evolution of the system obtained with a Gamma closure and the dashdotted line the evolution of the system with inverse Gamma closure. As initial condition we considered as initial condition $m_J(0) = 10$, $J \in \mathcal{C}$, and $\rho_I(0) = \rho_R(0) = 10^{-3}$, $\rho_S(0) = 1 - \rho_I(0) - \rho_R(0)$ and $\beta_1 = 0$, $\beta_2 = 10^{-5}$, $\gamma_I = 1/14$. From left to right we present the cases $\lambda = 10$ (left), $\lambda = 5$ (right).

In Figure 2 we depict the epidemic trajectories for several $\sigma^2 = 0.1, 0.2$ and fixed $\alpha = 1$, in all cases we considered as initial condition $m_J(0) = 10$ and $\rho_I(0) = \rho_R(0) = 10^{-3}$, $\rho_S(0) = 1 - \rho_I(0) - \rho_R(0)$. We may observe again that for larger λ the model obtained with inverse Gamma closure provides higher mean number of contacts for the infected population.

3 Control of the tail behaviour

In this section, we will explore the potential to control the dynamics of contact formation in a population, mimicking the role of non-pharmaceutical interventions (NPIs). These interventions aim to reduce the risk factors associated with the transmission of infectious diseases by influencing how individuals interact within the community.

The new kinetic description provides a powerful framework to analyse and quantify the impact of such measures. Specifically, it allows us to highlight the effects of policy-maker actions that directly target the contact distribution within the society. This approach is particularly valuable when only partial information about the population's contact patterns is available. By leveraging this mathematical approach, we seek to understand how modifying contact dynamics to mitigate the spread of an infection and guide the design of more effective intervention strategies.

In [29, 35], it has been shown that the design and implementation of selective policies can significantly influence the behaviour of contact distributions within a population. These selective policies are measures specifically tailored to act differentially on individuals based on their number of contacts, targeting specific subgroups rather than applying uniform interventions. The introduction of a penalization mechanism inversely proportional to the number of contacts can effectively alter the shape of the contact distribution. This approach enables a transition from a fat-tailed distribution, which is characterized by a high probability to find individuals with large number of contacts, to a slim-tailed distribution, such probability is negligible. This shift in the tail behaviour of the contact distribution has significant implications for public health strategies, as it suggests that selective interventions can play a crucial role in reducing the potential for super-spreading events and enhancing the overall effectiveness of non-pharmaceutical interventions in controlling disease transmission.

To this end, in the following we concentrate on the case $\delta = -1$ which produces inverse Gamma distributions (6) that are characterised by power-law tails. To steer the system towards a prescribed number of contacts we proceed as follows: we consider a simple control protocol resulting from the following minimization

$$\operatorname{argmin}_{u \in \mathcal{U}} \left[\frac{1}{2} \langle (x' - x_T)^2 \rangle + \frac{\nu}{2} u^2 \right], \quad (21)$$

where \mathcal{U} defines the class of admissible controls. The minimisation (21) is subject to the two possible dynamics that define the post-interaction state $x' \geq 0$. Hence, the minimisation of the cost in (21) can be obtained through a Lagrange

multiplier approach, see [4, 44]. In more detail, in the following we will consider the following transition laws:

A) Additively controlled transition

$$x' = x + \epsilon(\Psi(x/m_J)x + u) + x\eta. \quad (22)$$

Such class of controls have been classically considered in several constrained multiagent dynamics to enforce the emergence of prescribed patterns through the addition of external force in the dynamics, see e.g. [1, 4] and the references therein. In this case, the minimisation of (21) gives

$$u^* = -\frac{\epsilon}{\nu + \epsilon^2} ((x - x_T) + \epsilon\Psi(x/m_J)x)$$

which leads to the constrained interaction

$$x' = x + \frac{\nu\epsilon}{\nu + \epsilon^2}\Psi(x/m_J)x + \frac{\epsilon^2}{\nu + \epsilon^2}(x_T - x) + x\eta. \quad (23)$$

B) Interaction-driven controlled transition

$$x' = x + \epsilon\Psi(x/m_J)xu + x\eta, \quad (24)$$

which tries to modify the transition protocol of each single agent to steer the mean number of contacts towards $x_T > 0$. Hence, the minimisation of (21) gives

$$u^* = -\frac{\epsilon\Psi(x/m_J)x}{\nu + \epsilon^2(x\Psi(x/m_J))^2}(x - x_T).$$

and the constrained interaction is given by

$$x' = x - \frac{\epsilon^2(x\Psi(x/m_J))^2}{\nu + \epsilon^2(x\Psi(x/m_J))^2}(x - x_T) + x\eta. \quad (25)$$

This control has been introduced in [44] in a related modelling setting.

It is worth to notice that in both cases (22)-(24), in the limit $\nu \rightarrow 0^+$ we obtain an instantaneous control of the transition which is driven towards $x_T > 0$.

3.1 Fokker-Planck model and controlled equilibria

Proceeding as in Section 2.1 and by introducing the notation $f^{(A)}(x, t)$, $f^{(B)}(x, t)$ to denote the distribution of the number of contacts of a multiagent system characterised by microscopic constrained interaction expressed by the controls (A) and (B), respectively defined in (22) and (24), we obtain the evolution of observable quantities through the following space homogeneous Boltzmann-type equation

$$\frac{d}{dt} \int_{\mathbb{R}_+} \varphi(x) f^{(H)}(x, t) dx = \left\langle \int_{\mathbb{R}_+} (\varphi(x') - \varphi(x)) f^{(H)}(x, t) dx \right\rangle, \quad (26)$$

where $H = A, B$. By introducing the scaling of the penalization term $\nu \rightarrow \epsilon\nu$, in the quasi-invariant limit and for $\epsilon \rightarrow 0^+$, as observed in [44], we can obtain a Fokker-Planck-type equation with a modified drift term that takes into account the presence of the control. In terms of the controlled density $f^{(A)}(x, t)$, this equation reads

$$\begin{aligned} \partial_t f^{(A)}(x, t) = \\ \partial_x \left\{ \left[\frac{\alpha}{2\delta} \left(\left(\frac{x}{m_J} \right)^\delta - 1 \right) x + \frac{x - x_T}{\nu} \right] f^{(A)}(x, t) + \frac{\sigma^2}{2} \partial_x (x^2 f^{(A)}(x, t)) \right\} = \\ Q^{(A)}(f^{(A)})(x, t) \end{aligned} \quad (27)$$

which has the steady state

$$f^{(A),\infty}(x) = C_{\delta,\sigma^2,\alpha} x^{\frac{\lambda}{\delta} - 2 - \frac{2}{\sigma^2\nu}} \exp \left\{ -\frac{\lambda}{\delta^2} \left(\frac{x}{m_J} \right)^\delta - \frac{2}{\sigma^2\nu} \frac{x_T}{x} \right\}, \quad (28)$$

where the constant $C_{\delta,\sigma^2,\alpha} > 0$ is chosen such as the mass of the density is unitary. We observe that for any $\delta < 0$ the equilibrium distribution $f^{(A),\infty}$ is still a fat-tailed distribution and, therefore, the action of the control is not capable of modifying the tails of the distribution.

On the other hand, in terms of the density $f^{(B)}(x, t)$ the Fokker-Planck equation derived from (26) reads

$$\begin{aligned} \partial_t f^{(B)}(x, t) = \\ \partial_x \left\{ \frac{x^2}{\nu} \left[\frac{\alpha}{2\delta} \left(\left(\frac{x}{m_J} \right)^\delta - 1 \right) \right]^2 (x - x_T) f^{(B)}(x, t) + \frac{\sigma^2}{2} \partial_x (x^2 f^{(B)}(x, t)) \right\} = \\ Q^{(B)}(f^{(B)})(x, t) \end{aligned} \quad (29)$$

whose equilibrium distribution, for $\delta \neq -1$, $\delta \neq -1/2$, reads

$$f^{(B),\infty}(x) = C_{\delta,\sigma^2,\alpha} x^{-2} \exp \left\{ -\frac{2}{\sigma\nu} \left(\frac{\alpha}{2\delta} \right)^2 x L_\delta(x) \right\}, \quad (30)$$

with

$$L_\delta(x) = \left(\frac{x}{2\delta + 2} - \frac{x_T}{2\delta + 1} \right) \left(\frac{x}{m_J} \right)^{2\delta} + \left(\frac{2x_T}{\delta + 1} - \frac{2x}{\delta + 2} \right) \left(\frac{x}{m_J} \right)^\delta + \frac{x}{2} - x_T,$$

and $C_{\delta,\sigma^2,\alpha} > 0$ is a normalization constant. In the case $\delta \rightarrow -1$, the equilibrium density reads

$$f^{(B),\infty}(x) = C_{-1,\sigma^2,\alpha} x^{-2-\ell} \exp \left\{ -\frac{\alpha^2}{2\sigma^2\nu} \left[-(2m_J + x_T)x + \frac{x^2}{2} + \frac{m_J^2 x_T}{x} \right] \right\},$$

where $\ell = \frac{\alpha^2}{2\sigma^2\nu}(m_J^2 + 2x_T m_J)$. The obtained equilibrium density can be equivalently rewritten as follows

$$f^{(B),\infty}(x) = C_{-1,\sigma^2,\alpha} x^{-2-\ell} \mathcal{N}\left(2m_J + x_T, \frac{2\sigma^2\kappa}{\alpha^2}\right) \chi(x \geq 0) \times \exp\left\{-\frac{\alpha^2}{2\sigma^2\nu} \left[-\frac{(2m_J + x_T)^2}{2} + \frac{m_J^2 x_T}{x}\right]\right\}, \quad (31)$$

being $\chi(\cdot)$ the indicator function and $\mathcal{N}(\cdot, \cdot)$ a Gaussian distribution with mean defined in the first entry and variance in the second entry. Hence, in the case of the control (B) the equilibrium distribution exhibits slim tails.

Remark 3.1. *We may notice that the evolution of the controlled densities $f^{(H)}(x, t)$, $H = A, B$, is obtained in terms of the Fokker-Planck equations (27)-(29) which conserve only the mass. Hence, the momentum is not a conserved quantity for the presented control strategies.*

3.2 Controlled macroscopic equations

In this section we seek to obtain a closed system for the evolution of the main moments of the controlled kinetic system

$$\begin{cases} \partial_t f_S^{(H)}(x, t) = -K(f_S^{(H)}, f_I^{(H)})(x, t) + \frac{1}{\tau} Q_S^{(H)}(f_S^{(H)})(x, t), \\ \partial_t f_I^{(H)}(x, t) = K(f_S^{(H)}, f_I^{(H)})(x, t) - \gamma_I f_I^{(H)}(x, t) + \frac{1}{\tau} Q_I^{(H)}(f_I^{(H)})(x, t) \\ \partial_t f_R^{(H)}(x, t) = \gamma_I f_I^{(H)}(x, t) + \frac{1}{\tau} Q_R^{(H)}(f_R^{(H)})(x, t), \end{cases} \quad (32)$$

with $H = A, B$ and $Q^{(H)}(f^{(H)})(x, t)$ defined in (27) and (29). As observed in Remark 3.1, the only conserved quantity of the operators $Q^{(H)}(f^{(H)})$ is the mass.

To determine the evolution of mass fractions we integrate (32) to obtain the evolution of the controlled macroscopic equations. In the case $L = 1$ we get

$$\begin{aligned} \frac{d}{dt} \rho_S^{(H)} &= -\beta_1 \rho_S^{(H)} m_{1,S}^{(H)} \rho_I^{(H)} m_{1,I}^{(H)} \\ \frac{d}{dt} \rho_I^{(H)} &= \beta_1 \rho_S^{(H)} m_{1,S}^{(H)} m_{1,I}^{(H)} \rho_I^{(H)} - \gamma_I \rho_I^{(H)} \\ \frac{d}{dt} \rho_R^{(H)} &= \gamma_I \rho_I^{(H)} \end{aligned} \quad (33)$$

where, in the limit $\tau \rightarrow 0^+$, we recover the information on the constrained mean value as follows

$$m_{1,J}^{(H)} \rho_J^{(H)} \approx \rho_J^{(H)}(t) \int_{\mathbb{R}^+} x f_J^{(H),\infty}(x) dx.$$

being $f^{(H),\infty}(x, t)$ the steady state of the controlled problem which depends on the adopted control strategy, see (28)-(30)-(31). Therefore, the case $L = 1$ is

not sufficient to observe the behaviour of the tail distribution of the controlled contact formation dynamics.

On the other hand, in the case $L = 2$ we get

$$\begin{aligned}
\frac{d}{dt}\rho_S^{(H)} &= -\beta_1\rho_S^{(H)}m_{1,S}^{(H)}\rho_I^{(H)}m_{1,I}^{(H)} - \beta_2m_{2,S}^{(H)}\rho_S^{(H)}m_{2,I}^{(H)}\rho_I^{(H)} \\
\frac{d}{dt}\rho_I^{(H)} &= \beta_1\rho_S^{(H)}m_{1,S}^{(H)}m_{1,I}^{(H)}\rho_I^{(H)} + \beta_2m_{2,S}^{(H)}\rho_S^{(H)}\rho_I^{(H)}m_{2,I}^{(H)} - \gamma_I\rho_I^{(H)} \\
\frac{d}{dt}\rho_R^{(H)} &= \gamma_I\rho_I^{(H)}
\end{aligned} \tag{34}$$

where, as before, in the limit $\tau \rightarrow 0^+$, we can close the system through an equilibrium closure approach

$$\begin{aligned}
m_{1,J}^{(H)}\rho_J^{(H)} &\approx \rho_J^{(H)}(t) \int_{\mathbb{R}^+} x f_J^{(H),\infty}(x) dx \\
m_{2,J}^{(H)}\rho_J^{(H)} &\approx \rho_J^{(H)}(t) \int_{\mathbb{R}^+} x^2 f_J^{(H),\infty}(x) dx.
\end{aligned} \tag{35}$$

We observe that the control strategy (B), which ensures the contact distribution $f^{(B)}(x)$ in (30)-(31) is slim-tailed, consistently results in a finite second-order moment for the emerging controlled distribution. In contrast, control strategy (A) fails to guarantee the finiteness of the second-order moment for the corresponding controlled distribution, $f^{(A),\infty}(x)$ in (28). At the epidemic level, for large multiagent systems this indicates that interaction-driven controls are more effective than uniform-type controls in reducing the probability of finding agents with high number of contacts.

4 Numerical tests

In this section, we present several numerical results. In particular, in Test 1 we check for the long-time accordance between the numerical resolution of the Boltzmann-type equation (2) with binary interaction rules given by (1)-(23)-(25) in the quasi invariant limit, and the limiting Fokker-Planck equations (3)-(27)-(29). Numerical results, in both the uncontrolled and controlled scenario, are compared with the corresponding analytical equilibrium distributions. In Test 2 we investigate the behaviour of the tails of the contact distribution in the absence of epidemic exchange. We study the dependence of the different control strategies with respect to the penalization ν and the parameter λ . In Test 3 we check the consistency of the macroscopic limit, namely the accordance between the system (7) in the limit $\tau \rightarrow 0$ with $L = 2$, and the system (18)-(16) obtained with the moment closure described in Section 2.3. In Test 4 we numerically solve the system (32) for $H = A, B$ and different penalization and scale parameters. We compare the results with the uncontrolled scenario to study the effectiveness of the control strategies to reduce the spread of the epidemics.

The Boltzmann-type equation (2) with binary interaction rules given by (1)-(23)-(25) is solved with a classical DSMC scheme [42]. For the Fokker-Planck equations (1)-(23)-(25) in the absence of epidemic exchange, we adopt a structure-preserving (SP) implicit scheme, as proposed in [43]. To numerically solve the system, we rely on a time splitting technique [35]. In particular, we first rewrite the system in vector form

$$\frac{\partial \mathbf{f}^{(H)}}{\partial t}(x, t) = \mathbf{P}(x, \mathbf{f}^{(H)}(x, t)) + \frac{1}{\tau} \mathbf{Q}^{(H)}(\mathbf{f}^{(H)}(x, t)),$$

where $\mathbf{f}^{(H)} = \{f_J^{(H)}\}_J$ and $\mathbf{Q}^{(H)} = \{Q_J^{(H)}\}_J$, with $J = \{S, I, R\}$ and $H = A, B$, and \mathbf{P} is the vector representing the mass exchange between the compartments. Then, after discretizing the time domain with a step size $\Delta t > 0$ such that $t^n = n\Delta t$, we apply a first order in time splitting of the operators. Denoting by $\mathbf{f}^{(H),n}(x)$ an approximation of $\mathbf{f}^{(H)}(x, t^n)$ at the n -th time step, the splitting reads

$$\text{Fokker-Planck contact dynamics: } \begin{cases} \frac{\partial \mathbf{f}^{(H),*}}{\partial t} = \frac{1}{\tau} \mathbf{Q}^{(H)}(\mathbf{f}^{(H),*}) \\ \mathbf{f}^{(H),*}(x, 0) = \mathbf{f}^{(H),n}(x) \end{cases}$$

$$\text{Epidemic dynamics: } \begin{cases} \frac{\partial \mathbf{f}^{(H),**}}{\partial t} = \mathbf{P}(x, \mathbf{f}^{(H),**}) \\ \mathbf{f}^{(H),**}(x, 0) = \mathbf{f}^{(H),*}(x, \Delta t). \end{cases}$$

Finally, the solution at time t^{n+1} is $f^{(H),n+1}(x) = f^{(H),**}(x, \Delta t)$. The Fokker-Planck contact dynamics is solved with an implicit SP approach. The system of epidemic exchange is solved with a fourth order Runge-Kutta method.

4.1 Test 1: Boltzmann to Fokker-Planck

In this test, we consider the dynamic of a single Boltzmann-type equation in the quasi invariant collision limit to check for the accordance with the solution of the corresponding limiting Fokker-Planck equation. In more detail, we first compare equation (2), with binary rule (1), with (3), for both $\delta = +1, -1$. Then, we consider the controlled scenario with $\delta = -1$ and we solve (23)-(25) and (27)-(29), respectively. All the numerical results are also compared with the corresponding analytical equilibrium distribution.

We fix the parameters $\alpha = 1$, $\sigma^2 = 0.2$, $m_J = 5$, the x -domain $[0, 100]$, and $x_T = 3$, $\nu = 1$ for the controlled cases. For Maxwellian molecules corresponding to the case with $\delta = -1$, we choose $\Delta t = \epsilon = 0.01$, while for the non-Maxwellian case, i.e. $\delta = +1$, we fix $\epsilon = 0.01$ and we consider an upper bound for the kernel $B(\cdot)$ such that $\Delta t = \epsilon/10 = 0.001$. The time domain is $[0, T_f]$, with $T_f = 50$ in the uncontrolled case, and $T_f = 20$ in the controlled scenario. For the DSMC simulations, we consider $N = 10^6$ particles and a histogram reconstruction with

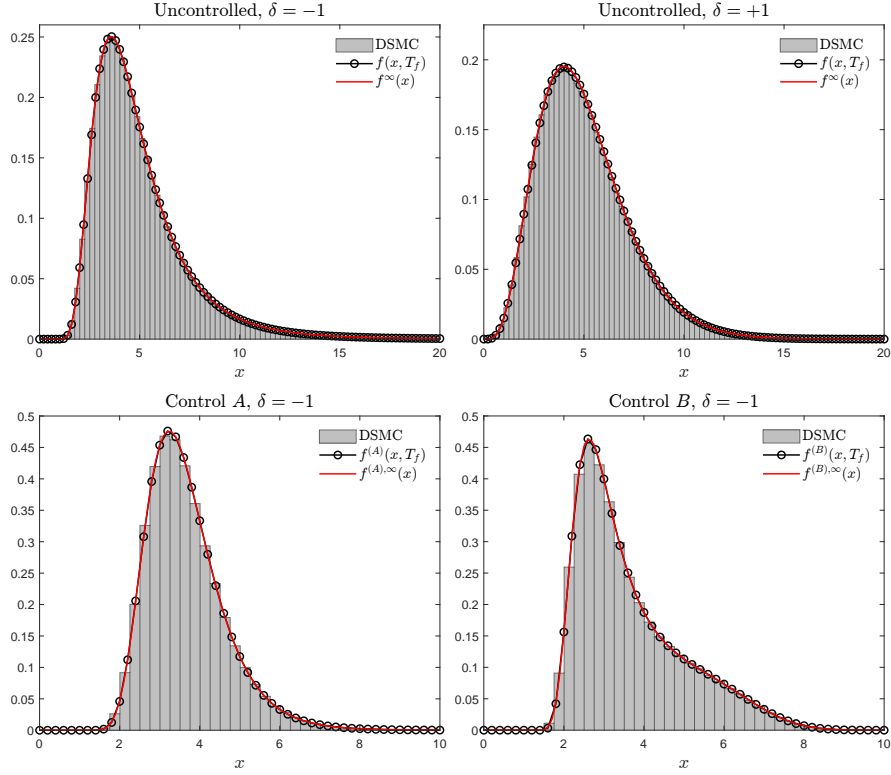


Figure 3: Comparison of the long-time behaviour of the numerical solution to the Boltzmann equations (grey bricks) in the quasi in variant interaction limit, the limiting Fokker-Planck equations (black circled lines), and the corresponding equilibrium distributions (solid red lines). Upper row: uncontrolled scenario with $\delta = -1$ (left), and $\delta = +1$ (right), with $T_f = 50$ in both cases. Bottom row: controlled scenario with strategies A (left) and B (right), for $\delta = -1$ and with $T_f = 20$ in both cases. The x -domain is $[0, 100]$, and it is cut for visualization purposes. The other parameters are $\alpha = 1$, $\sigma^2 = 0.2$, $m_J = 5$, $x_T = 3$, $\nu = 1$, $\Delta t = \epsilon = 0.01$ for $\delta = -1$, and $\Delta t = \epsilon/10 = 0.001$ for $\delta = +1$.

400 bins in the x -domain. For the resolution of the Fokker-Planck equation, we choose $\Delta x = 0.1$. The initial condition, in all the simulations, is a normalized uniform distribution $f(x, 0) = \mathcal{U}([6, 8])$.

In Figure 3 we may observe the accordance between the numerical solutions to the Boltzmann equations (grey rectangles) in the quasi in variant interaction limit, the limiting Fokker-Planck equations (black circled lines), and the corresponding equilibrium distributions (solid red lines).

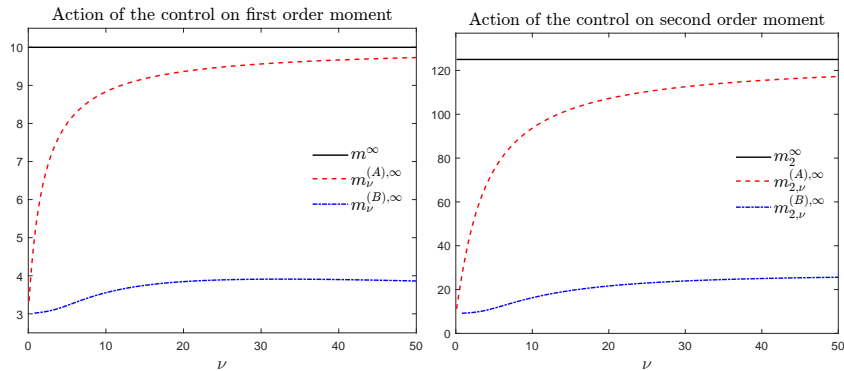


Figure 4: First (left) and second (right) order moment at the equilibrium versus the penalization coefficient ν . Solid black lines: uncontrolled scenario independent from the penalization coefficient, thus constant; dashed red lines: additive control strategy (A); dashdotted blue lines: multiplicative control strategy (B). The other coefficients are: $\delta = -1$, $\sigma^2 = 0.2$, $m = 10$, $x_T = 3$, and $\lambda = 3$.

4.2 Test 2: Tails behaviour of the contact distribution

In this subsection, we consider a single Fokker-Planck-type equation that describes the formation of the contact dynamics without epidemic exchange. We are interested in understand the tails behaviour in the presence of the control strategies (A) and (B), with respect to the penalization coefficient ν and the parameter $\lambda = \alpha/\sigma^2$. We concentrate on the case $\delta = -1$, since we have fat-tailed distribution at the equilibrium in the absence of the control. In all the tests, we fix the parameters $\delta = -1$, $\sigma^2 = 0.2$, $m = 10$, and $x_T = 3$.

In Figures 4-5, we also fix $\alpha = 0.4$ in a way that $\lambda = 2$, and we vary the penalization coefficient ν . In particular, in Figure 4 we show the first order moment m^∞ and $m_\nu^{(H),\infty}$ and the second order moment m_2^∞ and $m_{2,\nu}^{(H),\infty}$ at the equilibrium as a function of ν for the control strategies (A) and (B). Obviously, in the uncontrolled scenario there is no parametric dependence on ν and therefore the mean and the energy are constants. We may notice that, as ν decreases, for both the control strategies the mean approaches the same value, which is the selected target $x_T = 3$. We can also observe that the control (B) reduces at the equilibrium both the mean $m_\nu^{(H),\infty}$ and the energy $m_{2,\nu}^{(H),\infty}$ more than the control (A). In Figure 5, we observe the differences in the control of the tails of the distribution at the equilibrium $f^{(H),\infty}(x)$. In fact, as noticed in the previous sections, the control strategy (B) ensures that $f^{(B),\infty}(x)$ is a slim-tailed distribution, while the strategy (A) not. In these plots, we select $\nu = 1, 10$, and we look at the equilibrium distribution in semilogarithmic scale to highlight the behaviour of the tails.

Finally, in Figure 6 we fix the penalization coefficient $\nu = 1$ and the vary α with σ^2 fixed in a way that $\lambda = 2, 4$. As the value of λ decreases, the tails of the distribution increasingly exhibit their power-law behaviour. Consequently,

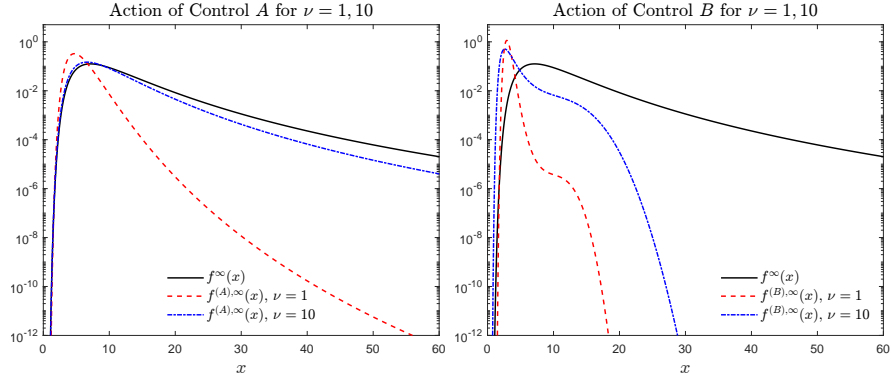


Figure 5: Contact distribution at the equilibrium for different penalization coefficients and control strategies. From left to right: $\nu = 1, 10$. In every plot the solid black line corresponds to the uncontrolled scenario $f^\infty(x)$, the dashed red lines to the additive control strategy A , $f^{(A),\infty}(x)$, and the dashdotted blue lines to the multiplicative control strategy B , $f^{(B),\infty}(x)$. The other coefficients are: $\delta = -1$, $\sigma^2 = 0.2$, $m = 10$, $x_T = 3$, and $\lambda = 2$.

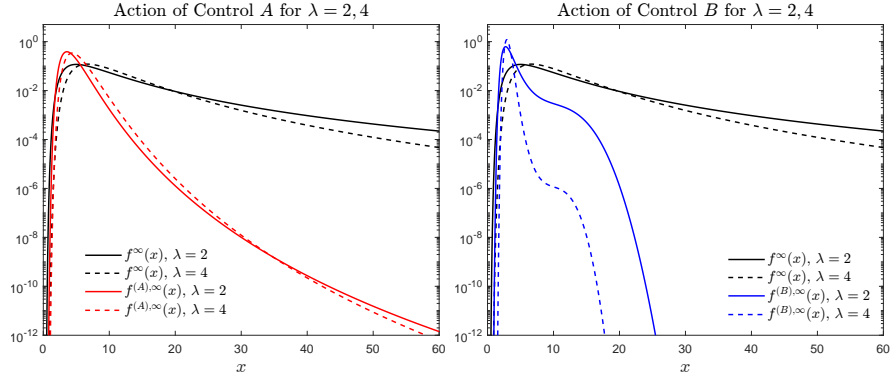


Figure 6: Contact distribution at the equilibrium for different coefficients $\lambda = 2, 4$ and control strategies A (left), and B (right). The other coefficients are: $\delta = -1$, $\sigma^2 = 0.2$, $m = 10$, $x_T = 3$, and $\nu = 1$.

for a fixed penalization coefficient ν , the control reduces them less.

4.3 Test 3: Consistency in the macroscopic limit without the control

In this test, we investigate numerically the consistency of the macroscopic closure of the kinetic system (7) with $L = 2$ and $\tau \rightarrow 0$ with the system of equations for the mass and first order moment (18)-(16). We choose the x -domain $[0, 500]$ discretized with step size $\Delta x = 0.02$, while the time domain is $[0, 20]$ with time

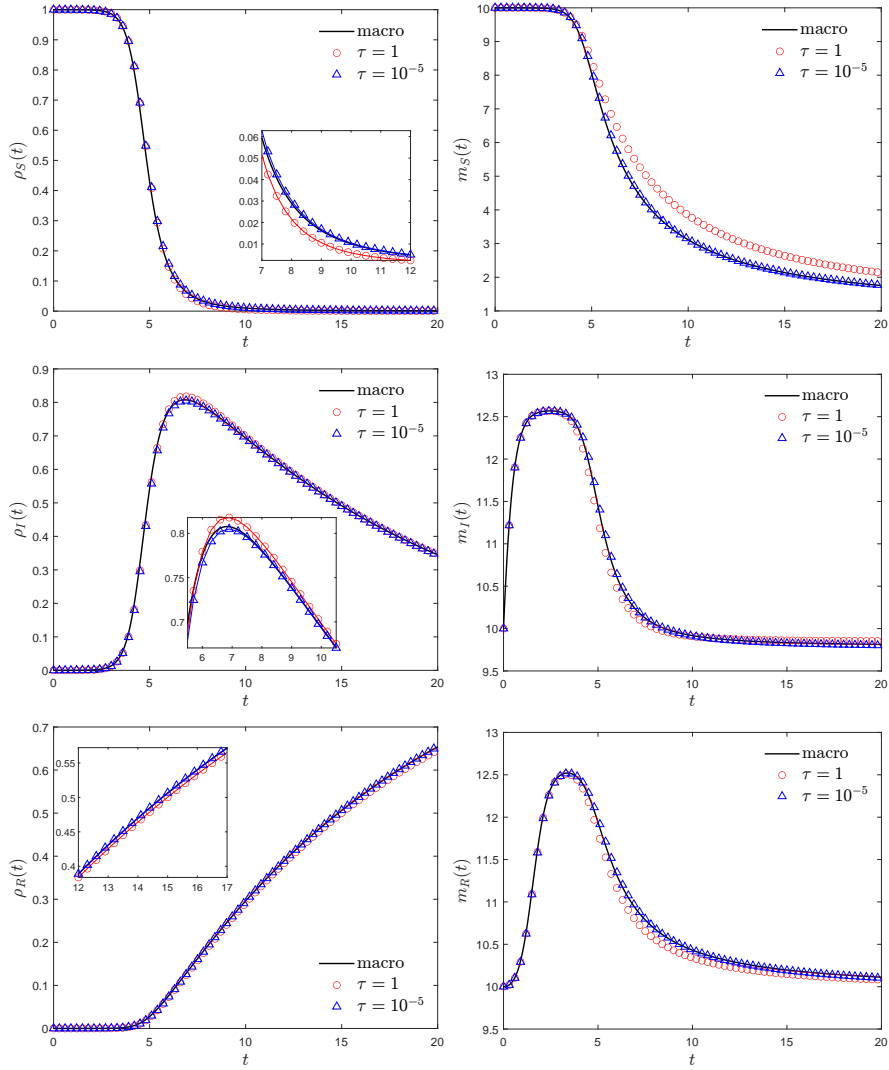


Figure 7: Time evolution of the mass fraction (left) and mean (right) of system (7) with $L = 2$, $\tau = 1$ (red circles) and $\tau = 10^{-5}$ (blue triangles), together with the solution of (18)-(16) (solid black lines). The epidemiological parameters are $\beta_1 = 2 \cdot 10^{-2}$, $\beta_2 = 2 \cdot 10^{-6}$, $\gamma = 1/14$, the other parameters are $\Delta x = 0.02$, $\Delta t = 0.01$, $\alpha = 1$, $\sigma^2 = 0.2$, in a way that $\lambda = 5$, and $\delta = -1$.

step $\Delta t = 0.01$. The epidemiological parameters are $\beta_1 = 2 \cdot 10^{-2}$, $\beta_2 = 2 \cdot 10^{-6}$, $\gamma = 1/14$, the other parameters are $\alpha = 1$, $\sigma^2 = 0.2$, in a way that $\lambda = 5$, and

$\delta = -1$. The initial distribution in every compartment J is

$$f_J(x, 0) = \rho_J(0) \frac{\lambda^\lambda}{(m_J^0)^\lambda \Gamma(\lambda)} x^{\lambda-1} \exp\left\{-\frac{\lambda x}{m_J^0}\right\}$$

with $m_J^0 = 10$ for every J , and initial masses $\rho_I(0) = \rho_R(0) = 10^{-5}$ and $\rho_S(0) = 1 - \rho_I(0) - \rho_R(0)$.

In Figure 7 we observe that in the limit $\tau \rightarrow 0^+$ we obtain a numerical evidence of the consistency between the derived macroscopic system and the kinetic model (7) with equilibrium closure approximation (18)-(16), as expected.

4.4 Test 4: The controlled system

In this test, we compare the effect of the different control strategies by numerically solve the system (32) with $H = A, B$. The adopted scheme is described at the beginning of Section 4 with $\Delta t = 0.01$ and $\Delta x = 0.02$ in the domain $[0, 500]$. The epidemiological parameters are $\beta_1 = 2 \cdot 10^{-2}$, $\beta_2 = 2 \cdot 10^{-6}$, and $\gamma_I = 1/14$. We choose in all tests $\delta = -1$, $\alpha = 1$ and $\sigma^2 = 0.2$, so that $\lambda = 5$. The initial conditions are

$$f_J(x, 0) = \rho_J(0) \frac{\lambda^\lambda}{(m_J^0)^\lambda \Gamma(\lambda)} x^{\lambda-1} \exp\left\{-\frac{\lambda x}{m_J^0}\right\}$$

with $m_J^0 = 10$ for every compartment J , and initial masses $\rho_I(0) = \rho_R(0) = 10^{-2}$ and $\rho_S(0) = 1 - \rho_I(0) - \rho_R(0)$.

In Figure 8, we solve the kinetic system (32) for several values of $\tau > 0$ and we compare the results with the unconstrained system with $L = 2$. In this test, we fix the penalization coefficient $\nu = 1$ and we compare the effect of the control strategies (A) and (B) for different scale parameter $\tau = 1, 10^{-5}$. We may observe how the control (B), while shaping the contact distribution in a slim-tailed distribution, is able to impact on the infection dynamics. On the other hand, the control (A) as it does not modify the structure of the contact distribution, which retains its overpopulated tail.

Conclusion

In this work, we focused on the macroscopic effects of kinetic control strategies applied to epidemic dynamics. We discussed the derivation of macroscopic models that describe the evolution of a controlled multi-agent system, obtained through an equilibrium closure approach. In more detail, we considered two control strategies previously proposed in the literature for similar models. Our results demonstrated how controlling the interaction strengths can transform a contact distribution with an overpopulated tail into a slim-tailed distribution, thereby reducing the heterogeneity in interactions. Additionally, we discussed the role of power-law tails in epidemic dynamics within the framework of the derived macroscopic models. Numerical results highlighted the effectiveness of

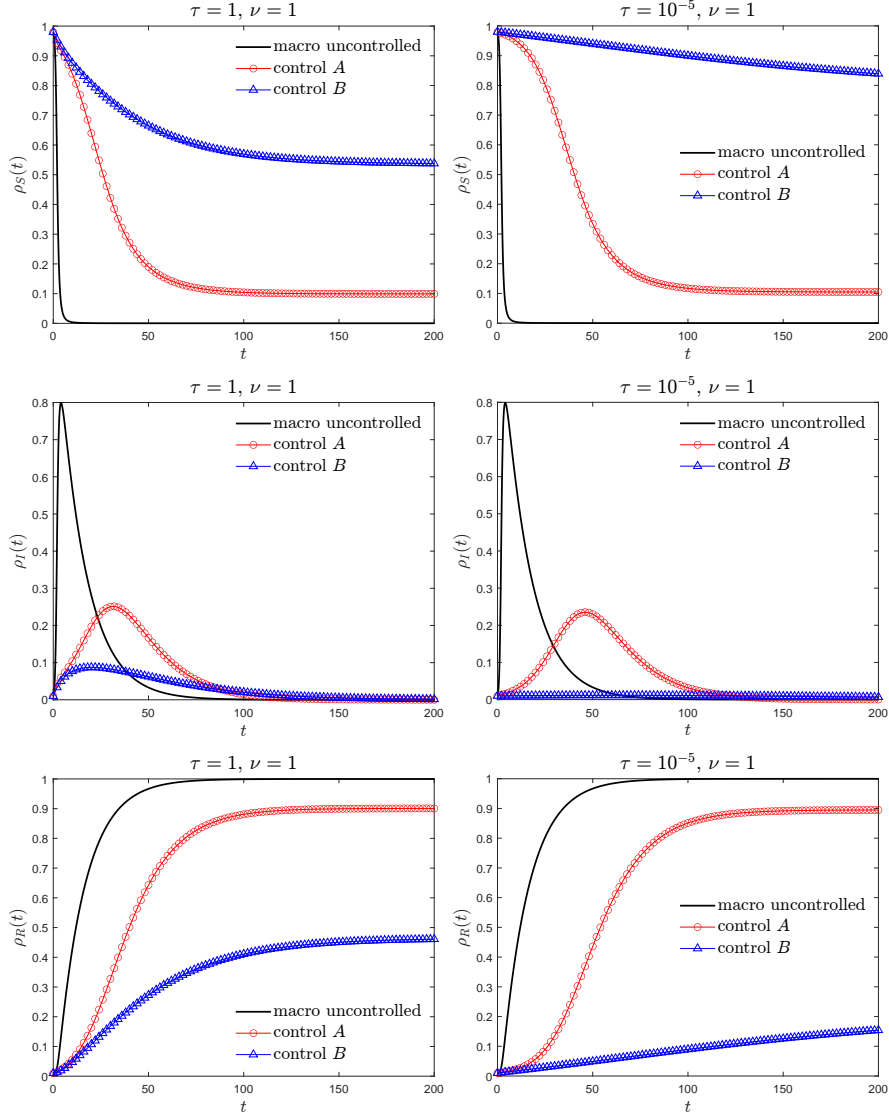


Figure 8: Time evolution of the mass fractions $\rho_J(t)$ in every compartment $J = \{S, I, R\}$. Left column: $\tau = 1$ and $\nu = 1$; right column: $\tau = 10^{-5}$ and $\nu = 1$. The black lines represent the uncontrolled scenario obtained by solving the system (18)-(16). The red circled lines is the control A obtained by solving the system (32) with $H = A$, the blue triangulated lines the control B, obtained by solving the same system with $H = B$. The epidemiological parameters are $\beta_1 = 2 \cdot 10^{-2}$, $\beta_2 = 2 \cdot 10^{-6}$, and $\gamma = 1/14$. Initial masses are $\rho_I(0) = \rho_R(0) = 10^{-2}$ and $\rho_S(0) = 1 - 2 \cdot 10^{-2}$. The other parameters are $\Delta t = 0.01$, $\Delta x = 0.02$ in the domain $[0, 500]$, $\delta = -1$, $\alpha = 1$ and $\sigma^2 = 0.2$.

the proposed approach in mitigating the spread of infection and demonstrated its potential for practical applications in epidemic control.

Acknowledgments

The work has been written within the activities of GNFM group of INdAM (National Institute of High Mathematics). A.M. was supported by the Advanced Grant Nonlocal-CPD (Nonlocal PDEs for Complex Particle Dynamics: Phase Transitions, Patterns and Synchronization) of the European Research Council Executive Agency (ERC) under the European Union’s Horizon 2020 research and innovation programme (grant agreement No. 883363). M.Z. acknowledges partial support by the MUR-PRIN 2020 project (No. 2020JLWP23) “Integrated Mathematical Approaches to Socio–Epidemiological Dynamics” and by European Union - NextGeneration EU.

References

- [1] G. Albi, Y.-P. Choi, M. Fornasier, D. Kalise. Mean Field Control Hierarchy. *Appl. Math. Optim.*, 76: 93–135, 2017.
- [2] G. Albi, M. Herty, L. Pareschi. Kinetic description of optimal control problems and applications to opinion consensus. *Commun. Math. Sci.*, 13(6): 1407–1429, 2015.
- [3] G. Albi, L. Pareschi. Selective model-predictive control for flocking systems. *Commun. Appl. Ind. Math.*, 9(2): 4–21, 2018.
- [4] G. Albi, L. Pareschi, G. Toscani, M. Zanella. Recent advances in opinion modeling: control and social influence. In *Active Particles Volume 1, Advances in Theory, Models, and Applications*, Eds. N. Bellomo, P. Degond, and E. Tadmor, Birkhäuser-Springer, 2017.
- [5] G. Albi, L. Pareschi, M. Zanella. Control with uncertain data of socially structured compartmental epidemic models. *J. Math. Biol.*, 82, 63, 2021.
- [6] G. Albi, L. Pareschi, M. Zanella. Modelling lockdown measures in epidemic outbreaks using selective socio-economic containment with uncertainty. *Math. Biosci. Eng.*, 18(6): 7161-7190, 2021.
- [7] R. M. Anderson, R. M. May. *Infectious Diseases of Humans: Dynamics and Control*. Oxford University Press: Oxford, 1991.
- [8] R. Bailo, M. Bongini, J. A. Carrillo, D. Kalise. Optimal consensus control of the Cucker-Smale model. *IFAC-PapersOnLine*, 51(13):1–6, 2018.
- [9] C. Bardos, F. Golse, D. Levermore. Fluid dynamic limits of kinetic equations. I. Formal derivations. *J. Stat. Phys.*, 63:323–344, 1991.

- [10] H. Behncke. Optimal control of deterministic epidemics. *Optim. Control Appl. Meth.*, 21: 269-285, 2000.
- [11] G. Béraud , S. Kazmerczak, P. Beutels, D. Levy-Bruhl, X. Lenne, N. Mielcarek, Y. Yazdanpanah, P.-Y. Boëlle, N. Hens, B. Dervaux. The French Connection: The First Large Population-Based Contact Survey in France Relevant for the Spread of Infectious Diseases. *PLoS One*, 10(7): e0133203, 2015.
- [12] M. Bisi, S. Lorenzani. Mathematical models for the large spread of a contact-based infection: A statistical mechanics approach. *J. Nonlin. Sci.*, 34: 84, 2024.
- [13] L. Bolzoni, E. Bonacini, C. Soresina, M. Groppi. Time-optimal control strategies in SIR epidemic models. *Math. Biosci.*, 292: 86-96, 2017.
- [14] S. Bonandin, M. Zanella. Effects of heterogeneous opinion interactions in many-agent systems for epidemic dynamics. *Netw. Heter. Media*, 19(1): 235-261, 2024.
- [15] F. Brauer. Mathematical epidemiology: Past, present, and future. *Infect. Dis. Model.*, 2(2):113-127, 2017.
- [16] M. Caponigro, M. Fornasier, B. Piccoli, E. Trélat. Sparse stabilization and optimal control of the Cucker-Smale Model. *Math. Control Relat. Fields*, 3(4):447-466, 2013.
- [17] J. A. Carrillo, D. Kalise, F. Rossi, E. Trélat. Controlling Swarms toward Flocks and Mills. *SIAM J. Contr. Optim.*, 60(3):1863-1891, 2022.
- [18] C. Cercignani. *The Boltzmann Equation and its Applications*, Springer Series in Applied Mathematical Sciences, vol. 67. Springer-Verlag, New York, NY.
- [19] A. Ciallella, M. Pulvirenti, S. Simonella. Kinetic SIR equations and particle limits. *Atti Accad. Naz. Lincei Cl. Sci. Fis. Mat. Natur.*, 32(2): 295-315, 2021.
- [20] F. Chiarello, B. Piccoli, A. Tosin. Multiscale control of generic second order traffic models by driver-assist vehicles. *Multiscale Model. Simul.*, 19(2):589-611, 2021.
- [21] Y.-P. Choi, D. Kalise, J. Peszek, A. A. Peters. A collisionless singular Cucker-Smale model with decentralized formation control. *SIAM J. Appl. Dyn. Syst.*, 18(4):1954-1981, 2019
- [22] G. Chowell, P. W. Fenimore, M. A. Castillo-Garsow, C. Castillo-Chavez. SARS outbreaks in Ontario, Hong Kong and Singapore: the role of diagnosis and isolation as a control mechanism. *J. Theor. Biol.*, 224(1):1-8, 2003.

- [23] R. M. Colombo, M. Garavello. Optimizing vaccination strategies in an age structured SIR model. *Math. Bios. Eng.*, 17(2):1074–1089, 2019.
- [24] R. M. Colombo, M. Garavello. A feedback strategy in hyperbolic control problems. In *Hyperbolic problems: theory, numerics, applications*, AIMS Ser. Appl. Math. Vol. 10: 377–384, 2020.
- [25] R. M. Colombo, F. Marcellini, E. Rossi. Vaccination strategies through intra-compartmental dynamics. *Netw. Heterog. Media*, 17(3):385-400, 2022.
- [26] R. Della Marca, N. Loy, A. Tosin. An SIR model with viral load-dependent transmission. *J. Math. Biol.*, 86(4):61, 2023.
- [27] G. Dimarco, L. Pareschi, G. Toscani, M. Zanella. Wealth distribution under the spread of infectious diseases. *Phys. Rev. E*, 102: 022303, 2020.
- [28] G. Dimarco, B. Perthame, G. Toscani, M. Zanella. Kinetic models for epidemic dynamics with social heterogeneity. *J. Math. Biol.*, **83**, 4, 2021.
- [29] G. Dimarco, G. Toscani, M. Zanella. Optimal control of epidemic spreading in the presence of social heterogeneity. *Phil. Trans. R. Soc. A*, 380:20210160, 2022.
- [30] W. Dong, K. Heller, A. Pentland. Modeling infection with multi-agent dynamics. In *Social Computing, Behavioral-Cultural Modeling and Prediction: 5th International Conference*, SBP 2012, College Park, MD, USA, April 3-5, 2012. Proceedings 5 (pp. 172-179). Springer Berlin Heidelberg.
- [31] S. Eubank, H. Guclu, V. Anil Kumar et al. Modelling disease outbreaks in realistic urban social networks. *Nature* 429, 180–184, 2004.
- [32] N. Ferguson, D. Cummings, S. Cauchemez, et al. Strategies for containing an emerging influenza pandemic in Southeast Asia. *Nat.*, 437: 209–214, 2005.
- [33] M. Fornasier, B. Piccoli, F. Rossi. Mean-field sparse optimal control. *Philos. Trans. R. Soc. Lond. Ser. A Math. Phys. Eng. Sci.*, 372(2028): 20130400, 2014.
- [34] M. Fornasier, F. Solombrino, F. Mean-field optimal control. *ESAIM Control Optim. Calc. Var.*, 20(4), 1123–1152, 2014.
- [35] J. Franceschi, A. Medaglia, M. Zanella. On the optimal control of kinetic epidemic models with uncertain social features. *Optim. Contr. Appl. Meth.*, 45(2): 494-522, 2024.
- [36] L. Fumanelli, M. Ajelli, P. Manfredi, A. Vespignani, S. Merler. Inferring the structure of social contacts from demographic data in the analysis of infectious diseases spread. *PLoS Comput. Biol.*, 8(9): e1002673, 2012.

- [37] N. Guglielmi, E. Iacomini, A. Viguerie. Identification of time delays in COVID-19 data. *Epidemiologic Meth.*, 12(1):20220117, 2023.
- [38] C. Le Bris, P.-L. Lions. Existence and uniqueness of solutions to Fokker-Planck type equations with irregular coefficients. *Commun. Partial Differ. Equ.*, 33(7):1272-1317, 2008.
- [39] S. Lee, G. Chowell, C. Castillo-Chavez. Optimal control for pandemic influenza: The role of limited antiviral treatment and isolation. *J. Theor. Biol.*, 265(2): 136-150, 2010.
- [40] N. Loy, A. Tosin. A viral load-based model for epidemic spread on spatial networks *Math. Biosci. Eng.*, 18(5):5635–5663, 2021
- [41] S. Merler, M. Ajelli. The role of population heterogeneity and human mobility in the spread of pandemic influenza. *Proc. R. Soc. B: 277:557–565*, 2010.
- [42] L. Pareschi, G. Toscani. *Interacting Multiagent Systems: Kinetic Equations and Monte Carlo Methods*. Oxford University Press, 2013.
- [43] L. Pareschi, M. Zanella. Structure preserving schemes for nonlinear Fokker-Planck equations and applications. *J. Sci. Comput.*, 74(3): 1575-1600, 2018.
- [44] L. Preziosi, G. Toscani, M. Zanella. Control of tumor growth distributions through kinetic methods. *J. Theor. Biol.*, 514: 110579, 2021.
- [45] A. Tosin, M. Zanella. Kinetic-controlled hydrodynamics for traffic models with driver-assist vehicles. *Multiscale Model. Simul.*, 17(2):716-749, 2018.
- [46] M. Salathé, M. Kazandjieva, J.W. Lee, P. Levis, M.W. Feldman, J.H. Jones. A high-resolution human contact network for infectious disease transmission. *Proc. Natl. Acad. Sci. U S A*, 107(51):22020-5, 2010.
- [47] R. Weightman, T. Akinode, B. Piccoli. Optimal control of pandemics via a sociodemographic model of non-pharmaceutical interventions. *Netw. Heter. Media*, 19(2):500–525, 2024.
- [48] M. Zanella. Derivation of macroscopic epidemic models from multi-agent systems. Preprint [arXiv:2410.08610](https://arxiv.org/abs/2410.08610), 2024.
- [49] M. Zanella, C. Bardelli, G. Dimarco, S. Deandrea, P. Perotti, M. Azzi, S. Figini, G. Toscani. A data-driven epidemic model with social structure for understanding the COVID-19 infection on a heavily affected Italian Province. *Math. Mod. Meth. Appl. Sci.*, 31(12):2533-2570, 2021.
- [50] J. Zhang et al. Changes in contact patterns shape the dynamics of the COVID-19 outbreak in China. *Science*, 368:1481–1486, 2020.